Mechanism of spontaneous excitability in human embryonic stem cell derived cardiomyocytes

Jonathan Satin[1], Izhak Kehat[2], Oren Caspi[2], Irit Huber[2], Gil Arbel[2], Ilanit Itzhaki[2], Janos Magyar[1], Elizabeth A. Schroder[1], Ido Perlman[2] and Lior Gepstein[2]

[1] *Department of Physiology, University of Kentucky College of Medicine, Lexington, KY 40536-0298, USA*
[2] *Department of Physiology and Biophysics, The Bruce Rappaport Faculty of Medicine and the Rappaport Family Institute for Research in the Medical Sciences. Technion-Israel Institute of Technology, Haifa, Israel*

Human embryonic stem cell-derived cardiomyocytes (hES-CMs) are thought to recapitulate the embryonic development of heart cells. Given the exciting potential of hES-CMs as replacement tissue in diseased hearts, we investigated the pharmacological sensitivity and ionic current of mid-stage hES-CMs (20–35 days post plating). A high-resolution microelectrode array was used to assess conduction in multicellular preparations of hES-CMs in spontaneously contracting embryoid bodies (EBs). TTX (10 μM) dramatically slowed conduction velocity from 5.1 to 3.2 cm s^{-1} while 100 μM TTX caused complete cessation of spontaneous electrical activity in all EBs studied. In contrast, the Ca^{2+} channel blockers nifedipine or diltiazem (1 μM) had a negligible effect on conduction. These results suggested a prominent Na^+ channel current, and therefore we patch-clamped isolated cells to record Na^+ current and action potentials (APs). We found for isolated hES-CMs a prominent Na^+ current (244 ± 42 pA pF^{-1} at 0 mV; $n = 19$), and a hyperpolarization-activated current (HCN), but no inward rectifier K^+ current. In cell clusters, 3 μM TTX induced longer AP interpulse intervals and 10 μM TTX caused cessation of spontaneous APs. In contrast nifedipine (Ca^{2+} channel block) and 2 mM Cs^+ (HCN complete block) induced shorter AP interpulse intervals. In single cells, APs stimulated by current pulses had a maximum upstroke velocity (dV/dt_{max}) of 118 ± 14 V s^{-1} in control conditions; in contrast, partial block of Na^+ current significantly reduced stimulated dV/dt_{max} (38 ± 15 V s^{-1}). RT-PCR revealed $Na_V1.5$, $Ca_V1.2$, and HCN-2 expression but we could not detect Kir2.1. We conclude that hES-CMs at mid-range development express prominent Na^+ current. The absence of background K^+ current creates conditions for spontaneous activity that is sensitive to TTX in the same range of partial block of $Na_V1.5$; thus, the $Na_V1.5$ Na^+ channel is important for initiating spontaneous excitability in hES-derived heart cells.

(Resubmitted 18 May 2004; accepted after revision 2 July 2004; first published online 8 July 2004)
Corresponding author L. Gepstein: Cardiovascular Research Laboratory, The Bruce Rappaport Faculty of Medicine, Technion-Israel Institute of Technology, 2 Efron Street, P.O.B. 9649, 31096 Haifa, Israel. Email: mdlior@tx.technion.ac.il

Human embryonic stem cells are capable of unlimited proliferation in culture in the undifferentiated state and under the proper conditions can differentiate into different cell types including spontaneously beating cardiac myocytes (Kehat *et al.* 2001, 2002). Spontaneous beating or automaticity is not normally exhibited by mature atrial or ventricular myocytes. In contrast, embryonic heart cells display spontaneous activity (DeHaan & Gottlieb, 1968). The main requirement for automaticity is the presence of inward current at diastolic potentials. Although two recent reports of human embryonic stem cell-derived cardiac myocytes (hES-CMs) document action potentials (He *et al.* 2003; Mummery *et al.* 2003), there are no studies of ionic currents in hES-CMs. Moreover, the more thoroughly studied mouse ES-derived CMs exhibit AP morphologies that broadly reflect either atrial-like, ventricular-like, or nodal-like parameters (Hescheler *et al.* 1999; Sachinidis *et al.* 2003) that differ markedly from their human counterparts.

The cardiac Na^+ channel (termed $Na_V1.5$) is expressed in relatively high density on surface membrane of mature heart cells in atria and ventricle. Despite the high $Na_V1.5$ expression these cell types are not normally automatic because a high density of inward rectifier K^+ channels (Kir) clamps the membrane potential to a value near the K^+ reversal potential. At such hyperpolarized potentials

 DOI: 10.1113/jphysiol.2004.068213

the $Na_V1.5$ channel's open probability approaches 0. In quiescent, mature heart cells, the initiating depolarization originates from neighbouring cells via gap junctions. Depolarization of membrane potential (V_m) activates $Na_V1.5$ rapidly, driving the rapid AP upstroke, and within a few milliseconds of sustained depolarization $Na_V1.5$ inactivates. Thus, $Na_V1.5$ serves the role of generating a pathway for a rapid influx of depolarizing current. The maximum diastolic potential (MDP) is a key control point for $Na_V1.5$, if MDP is relatively depolarized then $Na_V1.5$ will be largely inactivated and unable to contribute to the AP upstroke. For this reason, there is a correlation between Na^+ channel current density (not simply channel density), and the maximum upstroke velocity of the cellular AP (dV/dt_{max}). Moreover, in the developing heart there is a an increase in dV/dt_{max} from < 20 to 100–150 V s^{-1} that is concomitant with the onset of TTX sensitivity (McDonald *et al.* 1973), an increase in Na^+ current density (Fujii *et al.* 1988), and a negative shift in the MDP (McDonald *et al.* 1973; DeHaan, 1980; Sperelakis, 1984).

Given the exciting potential use of hES-CMs as replacement tissue in diseased heart (Gepstein, 2002; Kehat & Gepstein, 2003), and as an *in vitro* model for the study of early human cardiac development it is important to characterize their functional properties. We assessed the electrical properties of these cells in spontaneously beating embryoid bodies (EBs) using a multielectrode array mapping technique and detailed patch-clamp recordings and pharmacologically dissected the critical pathways in these structures. Our results provide the first description of the ionic currents in hES-CMs and show that the basis for spontaneous electrical activity in these cells is the absence of Kir conductance, a phenomenon that provides the substrate for a relatively large voltage-gated Na^+ current to drive activity.

Methods

Human ES cell culturing and production of EBs

Human undifferentiated ES cells of the clone H9.2 (Amit *et al.* 2000) were grown on mouse mitotically inactivated (mitomycin C) embryonic fibroblast feeder layer as previously described (Amit *et al.* 2000; Kehat *et al.* 2001). To induce differentiation, hES cells were cultured in suspension for 7–10 days, where they aggregated to form EBs. At 22–35 days, beating areas were either plated on gelatin, or fibronectin-coated microelectrode array plates or dispersed into isolated cells for the patch-clamp studies.

Multielectrode array (MEA) mapping technique

Extracellular recordings from the EBs were performed with a MEA data acquisition system as previously described (Feld *et al.* 2002; Kehat *et al.* 2002). During the recording sessions, the MEA was constantly perfused with a gas mixture consisting of 5% CO_2 and 95% air, at a temperature of $37.0 \pm 0.1^{\circ}$C.

Local activation time (LAT) at each electrode was determined as the timing of the maximal negative intrinsic deflection (dV/dt_{min}) of the unipolar recording. The measured LATs at all electrodes were then used for generation of colour-coded activation maps. Local conduction velocity vector fields were determined from these maps, as previously described (Kehat *et al.* 2002).

Following baseline recording, 20 μl of stock solution of the test drug were added to the 2 ml of culture medium. The pharmacological agents included tetrodotoxin (TTX; Alomone Laboratories, Jerusalem, Israel) at final concentrations of 10 or 100 μmol l^{-1}, and diltiazem hydrochloride (1 or 10 μmol l^{-1}, Sigma, St Louis, MO, USA). Extracellular recordings were performed for 30 s, at baseline and 5 min following drug application. The effects of these drugs on conduction were evaluated by examining the culture's global velocity (measured as the distance between earliest and latest activation divided by the total MEA activation time), the mean magnitude of the local velocity vector, and the maximal absolute value of the first time derivative of the extracellular signal.

Electrophysiological recordings

For single cell AP and ionic current, the whole-cell configuration of the patch-clamp technique was used. After dissociation cells were replated for 1–4 days on gelatin, or fibronectin-coated glass cover slips. The patch pipette solution consisted of (mM): 120 KCl, 1 $MgCl_2$, 3 Mg-ATP, 10 Hepes, 10 EGTA (pH 7.3). The bath recording solution consisted of (mM): 140 NaCl, 5.4 KCl, 1.8 $CaCl_2$, 1 $MgCl_2$, 10 Hepes, 10 glucose (pH 7.4). Upon seal formation and following patch break, analog capacitance compensation was used. APs were recorded from the current-clamp mode. Voltage recordings were filtered at 10 kHz. For voltage-clamp experiments only isolated cells were selected. Series resistance compensation was used up to 80%, and was monitored immediately prior to the initiation of each individual protocol. Currents were filtered at 10 kHz and sampled at 20 or 50 kHz. Axopatch 200B, Digidata1322, and pClamp8 (Axon, Burlingame, CA, USA) was used for data amplification, acquisition, and analysis. Only spontaneously beating cells were chosen for study as a positive identifier of heart muscle. For consideration of voltage control, roughly spherical cells were chosen (see Fig. 2 below), and the mean cell capacitance (C_m) of 21.6 ± 1.3 pF ($n = 68$) is small relative to C_m of typical mature heart cells. For current–voltage curves (activation curves) data were discarded for recordings showing indications of inadequate voltage that included an apparent threshold voltage for Na^+ current activation, or activation that was described by a Boltzmann distribution with a slope factor

Table 1. Sequences of PCR primers and real time probes (human)

Target sequence	Forward primer (5′-3′)	Reverse primer (5′-3′)	Accession no.
$Ca_v1.2$	gagaacagcaagtttgactttgacaa	cgaaggtggagacggtgaa	NM_000719
$Ca_v1.3$	tccaaggagacgcctactacct	gcgcaggcactcaaagttg	NM_000720
$Na_V1.5$	catcttcacaggcgagtgtattg	gatattccagctgttggtgaagtagta	AF482988
Kir2.1	tcacggctgccttcctctt	tccgtgacatctgaaacca	U16861
Kir2.3	tgtcgcccatcatcattgtc	tccttgcccatgccataaa	NM_004981
GAPDH	cctgttcgacagtcagccg	cgaccaaatccgttgactcc	BC014085
HCN-2	cgcctgatccgctacatccat	agtgcgaaggagtacagttcact	AF065164
HCN-4	cccgcctcattcgatatattcac	gagcgcgtaggagtactgcttc	AJ132429

steeper than 4. Although this is a rather steep voltage dependence, other protocols indicated adequate voltage control. For steady-state inactivation and recovery from inactivation protocols the currents elicited by common test potentials had indistinguishable kinetics independent of current amplitude. For HCN recordings current was filtered at 2 kHz and a split clock was used to sample at 10 kHz and 1 kHz to prolong the duration of the test step. All recordings were performed at 26–29°C. Individual voltage protocols are indicated as insets in the figures. Equations used for fitting data are presented in the figure legends. Curve fitting was performed with either Clampfit8 or non-linear curve fitting routines in Origin7.1.

Real-time PCR

Real-time PCR was performed in 96-well optical plates in triplicate. Samples were prepared using Brilliant Sybr Green QPCR Master Mix (Stratagene). Primers used are shown in Table 1. Fetal human heart cDNA (0.1 ng Stratagene) or 0.1 ng experimental cDNA was used as a template in the real-time PCR reactions. Experimental cDNA was obtained from RT of total RNA isolated from beating EBs trimmed from non-beating areas to enrich the preparation in cardiac myocytes. EBs plated for 25–30 days were used for total RNA isolation. PCR samples were cycled for 50 cycles using an ABI 7700 Sequence Detector (Applied Biosystems). Default 7700 cycle conditions were as follows: 15 min at 95°C followed by 50 cycles of 15 s at 95°C, 30 s at 62°C and 30 s at 72°C. A standard curve was generated from dilutions of the human fetal heart cDNA by plotting the natural log of the threshold cycle (C_T) against the natural log of the number of molecules. The C_T was defined as the cycle at which a statistically significant increase in the magnitude of the signal generated by the PCR reaction was first detected. C_T was calculated under default settings for the real-time sequence detection software (Applied Biosystems). To maximize accuracy, dilutions were made over the range of copy numbers that included the amount of target cDNA expected in the experimental cDNA samples. Specific calcium and sodium channel component cDNA molecules present in the experimental cDNA were calculated from the standard curve (Bustin, 2002; Whelan *et al.* 2003). To rule out contaminating genomic DNA a 'no RT' control was performed for each sample. Dissociation plots showed no evidence of primer-dimer and non-specific PCR products.

Results

hES-CM conduction and automaticity is TTX sensitive

We have previously shown that spontaneously contracting areas could be generated within EBs during the *in vitro* differentiation of the H9.2 human ES cell line. We have also demonstrated using a multielectrode array mapping technique and detailed immunostaining studies that these beating areas are comprised of an isotropic cardiomyocyte cell network acting as a functional syncytium with stable spontaneous pacemaking activity and synchronous AP propagation (Kehat *et al.* 2002).

The spontaneous activity and the relatively rapid conduction in these studies suggested the presence of a high-density inward current via voltage-activated channels. Therefore, we first tested the effects of Na^+ channel and Ca^{2+} channel blockers on spontaneous activity and conduction. A representative MEA recording of electrical activity from a beating cluster is shown in Fig. 1*A* and *B*. Note the relative fast conduction with a total activation time of 11.5 ms in this example. Similar conduction profiles were manifested in all EBs tested in control bath solution.

The relatively rapid conduction implicates the presence of functional Na^+ channels. Therefore, we tested the effect of the selective Na^+ channel blocker TTX on the excitable properties of this tissue. Figure 1*C* and *E* shows the effect of application of 3 μM (*C*) and 10 μM (*E*) TTX in one of the EBs studied. Note the significant slowing of conduction with total activation time increasing from the baseline value of 11.5 ms to 14 ms (*C*) to 35 ms (*E*). Note also that in some of the EBs, TTX application resulted also in the generation of local conduction blocks (arrows in Fig. 1*E*). At 10 μM,

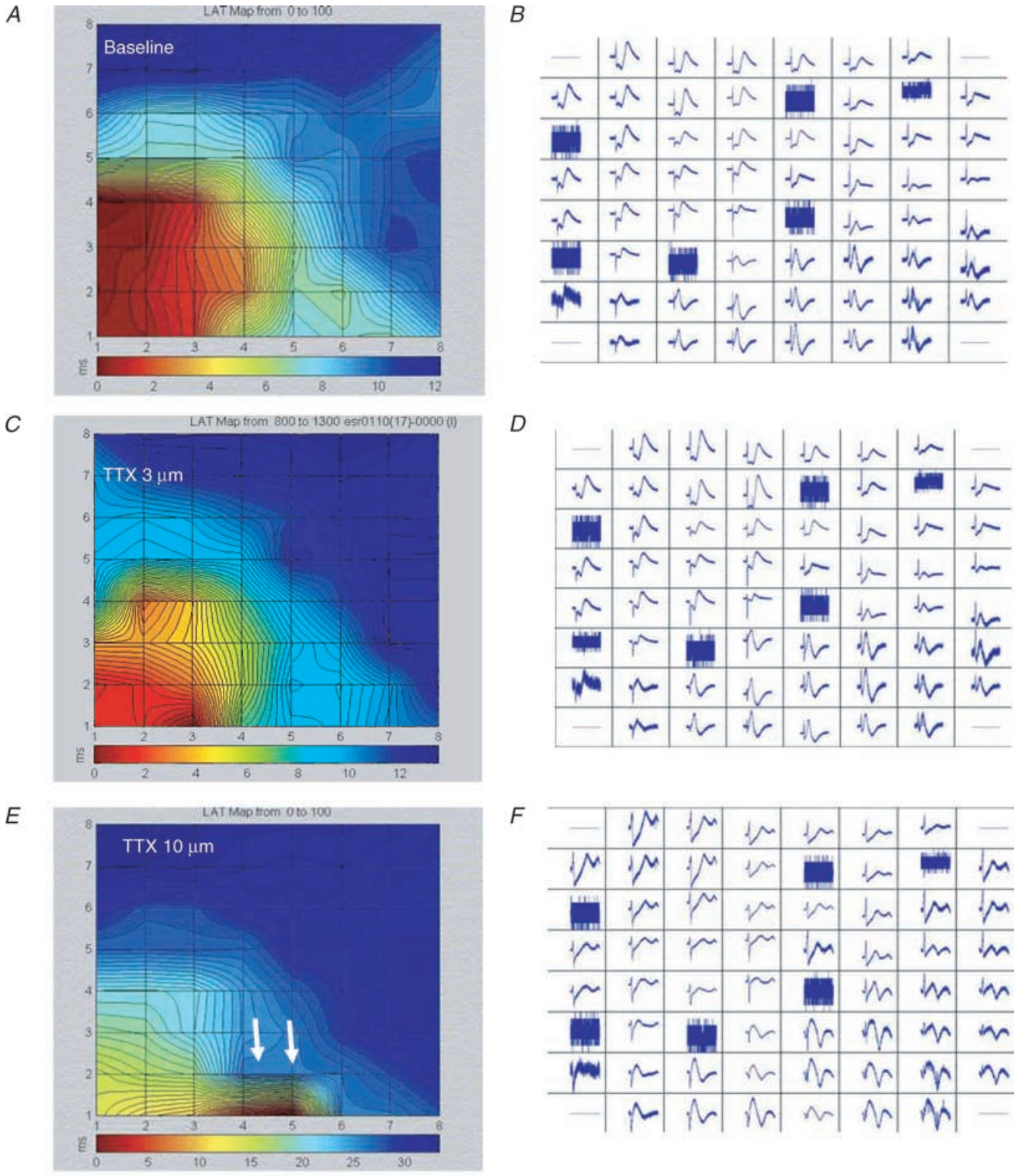

Figure 1. MEA – Na^+ channel block, but not Ca^{2+} channel block slows conductionb
A and *B*, simultaneous extracellular tracings from all 60 electrodes (*B*) recorded from a beating EB and the resulting high-resolution activation map (*A*) as generated by the MEA mapping technique, during baseline recordings. *C–F*, extracellular recordings (*D*,*F*) and activation maps (*C*,*E*) generated from the same EB following application of 3 μM (*C*,*D*) and 10 μM (*E*,*F*) TTX. Note the increase in total MEA activation time from a baseline value of 11.5 ms to 14.0 ms (*C*) to 35.0 ms (*E*). In some of the EBs application of TTX (10 μM) also resulted in the generation of local conduction blocks (white arrows).

TTX slowed conduction in all the EBs studied from a mean conduction velocity vector of 5.1 ± 6 cm s^{-1} at baseline to 3.2 ± 3 cm s^{-1} ($P < 0.05$). This concentration also slowed the spontaneous beating rate of the EBs from 1.14 ± 0.62 to 0.74 ± 0.24 Hz ($P = 0.031$, Wilcoxon signed rank test) and eventually stopped automaticity in two out of the six EBs studied. At 100 μM, TTX blocked all spontaneous activity in the additional three EBs. In contrast to TTX, the Ca^{2+} channel blocker diltiazem (at 1 or 10 μM), or nifedipine (at 0.1 or 1 μM) neither slowed nor blocked AP conduction and had no effect on automaticity. These results suggest that Na^+ channels, but not Ca^{2+} channels, are essential for initiation and efficient conduction of APs through the hES-CM syncytium.

Syncytial APs inhibited by Na^+ channel, but not Ca^{2+} channel blockade

Our next step was to evaluate the action potential properties of the hES-CMs and the response to Na^+ channel and Ca^{2+} channel blockade in clusters of spontaneously beating hES-derived cells. Figure 2*A* depicts a typical cluster of hES-CMs. This photograph shows the pattern of growth of a spontaneously contractile syncytium of cells. The partially dispersed cells that remain in clusters tend to grow vertically and at the periphery of these clusters individual, roughly spherical cells are accessible to patch electrodes. In all clusters tested, the cells within a cluster were beating in synchrony. Figure 3 shows representative spontaneous, rhythmic APs from a cluster of spontaneously contractile tissue. In clusters of cells under control conditions the rhythm was regular (Fig. 3*A*). The AP morphology (Fig. 3*B*) consisted of a rapid upstroke followed by a plateau phase. Upon repolarization, there was a slow, spontaneous depolarization. At 3 μM, TTX converted cluster APs from a single diastolic depolarization rate (DDR) to a biphasic DDR (Fig. 3*C*). As a consequence of an additional slow DDR the interpulse interval (beat rate) of cluster was slowed (Fig. 3*D*). Also, the maximal upstroke velocity (dV/dt_{max}) was slowed by Na^+ channel block by 3 μM TTX. In contrast, we could not detect any significant effects on action potential durations (APD) by 3 μM TTX (Fig. 3*F*). At 10 μM, TTX completely inhibited spontaneous activity (Fig. 3*G*). This effect was readily reversed upon wash-out (Fig. 3*G*). We conclude that Na^+ channel current contributes to both the AP upstroke and the spontaneous diastolic 'pacemaker' depolarization.

The AP morphology of hES clusters shows that this heart tissue has robust pacemaker function. In mature cardiac pacemaker cells, voltage-gated Ca^{2+} channels are important contributors to spontaneous depolarization and the upstroke of the action potential. Surprisingly, we noted that cardiac L-type Ca^{2+} channel blockade had little effect on conduction. Similarly, 100 nM nifedipine had no effect on AP spontaneous activity; however, 1 μM nifedipine had two obvious effects on cluster APs (Fig. 4). The rate of spontaneous diastolic depolarization was increased (Fig. 4, compare panels *A* and *C*), and the APD was dramatically shortened (Fig. 4, compare panels *B* and *D*). Underlying the nifedipine-induced increased spontaneous beat rate was an increased DDR. TTX slowed DDR but had minimal effects on APD. In contrast, nifedipine shortened APD, and we therefore interpret this resulting speeding of DDR as secondary to APD shortening. The shorter APD translates into a briefer refractory period, and in turn additional available Na^+ current. We next conducted single cell experiments which provided additional supporting data for our straightforward hypothesis that Na^+ channel current is a major contributor to both the upstroke and pacemaker depolarization phases of the hES heart cells.

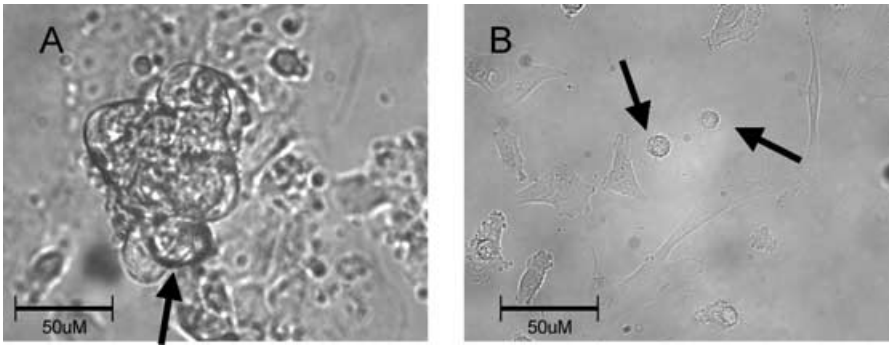

Figure 2. Representative beating cell clusters and isolated cells
A shows all the cells within the cluster contracting in synchrony suggesting entrainment of cells electrical activity. Note the typical pattern of growth that includes cells growing vertically. Arrow shows a common approach angle for patch electrode to a cell on the periphery of the beating cluster. *B*, single cells chosen for study, indicated by arrows, beat spontaneously and were roughly spherical with a slightly splayed, flat attachment to the coverslip. Both photographs acquired with 40× objective lens.

ES-CM single cell background currents: functional expression of the pacemaker current HCN, but no detectable functional expression of Kir

Cardiac pace-making tissue such as mature nodal cells or embryonic myocardium has relatively high input resistance as a consequence of the diminished expression of background K^+ currents, principally those of the inward rectifier family Kir2. To measure background current we voltage-clamped isolated, single hES-CMs. Figure 2*B* depicts typical single cells in isolation. The cell shape was roughly spherical and small (cell capacitance ranged from 7 to 40 pF), making them amenable to improved spatial voltage control. All cells selected for study were spontaneously contractile. Voltage steps from a holding potential (V_{hold}) of −40 mV to potentials negative to −70 mV elicited slowly developing inward current (Fig. 5). The Kir channel is sensitive to external Ba^{2+} with a half-block concentration on the order of 20 μM (Hille, 2001), but in hES cells 0.5 mM Ba^{2+} had no effect on ionic current (Fig. 5*B* and *D*). Also, there was inward current at the potassium reversal potential ($E_K \sim -84$ mV; Fig. 5*C*), which indicated that the current observed was not via K^+-selective Kir channels. Taken together there is no evidence for detectable Kir in hES-CMs differentiated for less than 42 days.

The slow rate of activation and inward current positive to E_K is suggestive of the HCN channel current. To test for HCN we tested the effect of 2 mM Cs^+ on this hyperpolarization-activated current.

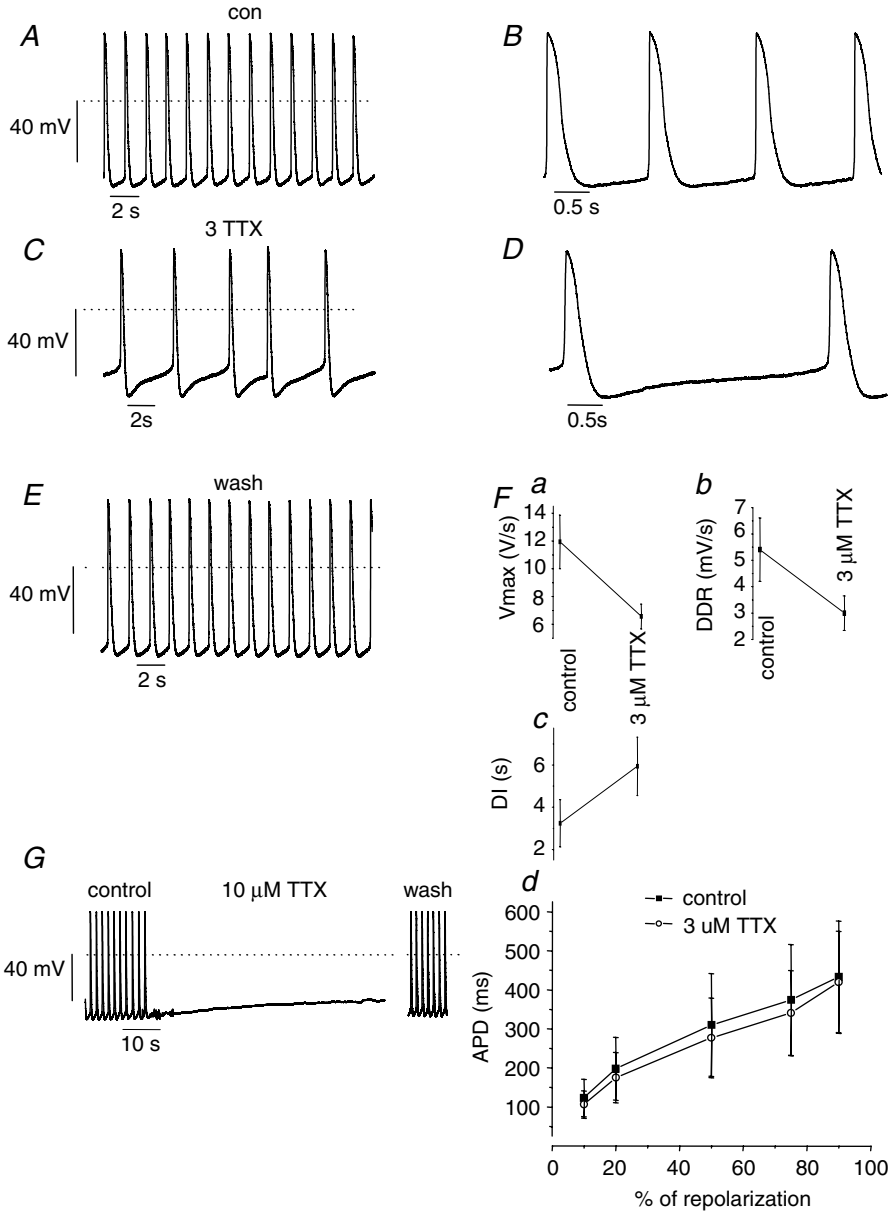

Figure 3. Action potentials from cell clusters are sensitive to TTX
A and *B*, APs from a representative cluster in control bath solution. Note that the AP rhythm was regular. *B*, expanded view of *A* to illustrate AP morphology. Dotted line indicates 0 mV. *C* and *D*, 3 μM TTX slowed spontaneous rate of AP initiation. *D*, expanded view of *C*; in comparison to control (*A*) the major effect of 3 mM TTX was to slow the spontaneous diastolic depolarization. *E*, washout of TTX shows the effects are reversible. *F*, summary data from 6 recordings shows that 3 μM TTX: (*a*) slowed the maximum upstroke velocity (V_{max}), (*b*) slowed the diastolic depolarization rate (DDR), and (*c*) prolonged the diastolic interval. All the effects were statistically significant ($P < 0.01$). *Fd*, APD is plotted as a function of the time required for 10, 20, 50, 75 and 90% of repolarization. Control APD (■) tended to be shorter than APD in the presence of TTX (○), but the differences were not significant. $n = 6$ for all panels. *G*, APs from a representative cluster in control, 10 μM TTX and following washout. 10 μM TTX induced quiescence and was accompanied by a slow steady depolarization to ∼−40 mV. Note break in time scale due to relative prolonged washout duration.

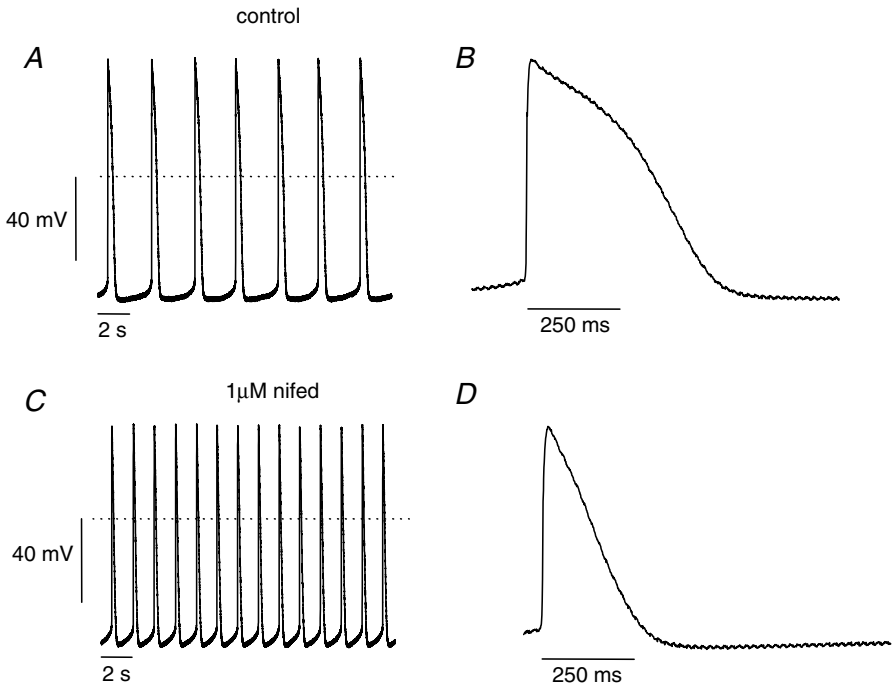

Figure 4. Nifedipine does not inhibit spontaneous APs
A and *B*, representative recordings of spontaneous APs from a cell cluster in control bath solution. *C* and *D*, 1 μM nifedipine increases spontaneous AP rate. *B* and *D* show traces on an expanded time scale to highlight effects of nifedipine. Although 1 μM nifedipine did not block spontaneous AP activity it dramatically shortened APD as expected from Ca^{2+} channel blockade.

Figure 6 shows that 2 mM Cs^+ completely blocks hyperpolarization-activated current. The time course of activation of the HCN-like current was voltage dependent, with slower rates at more depolarized potentials (Fig. 6*D*). In addition to demonstrating HCN expression, the raw current traces in Fig. 6*A* and *B* illustrate an important mechanism underlying pacing. The duration of the various hyperpolarizing voltage steps was ~2.3 s. At the end of the hyperpolarization a large fast inward current is elicited upon return to −40 mV, but only for hyperpolarizing

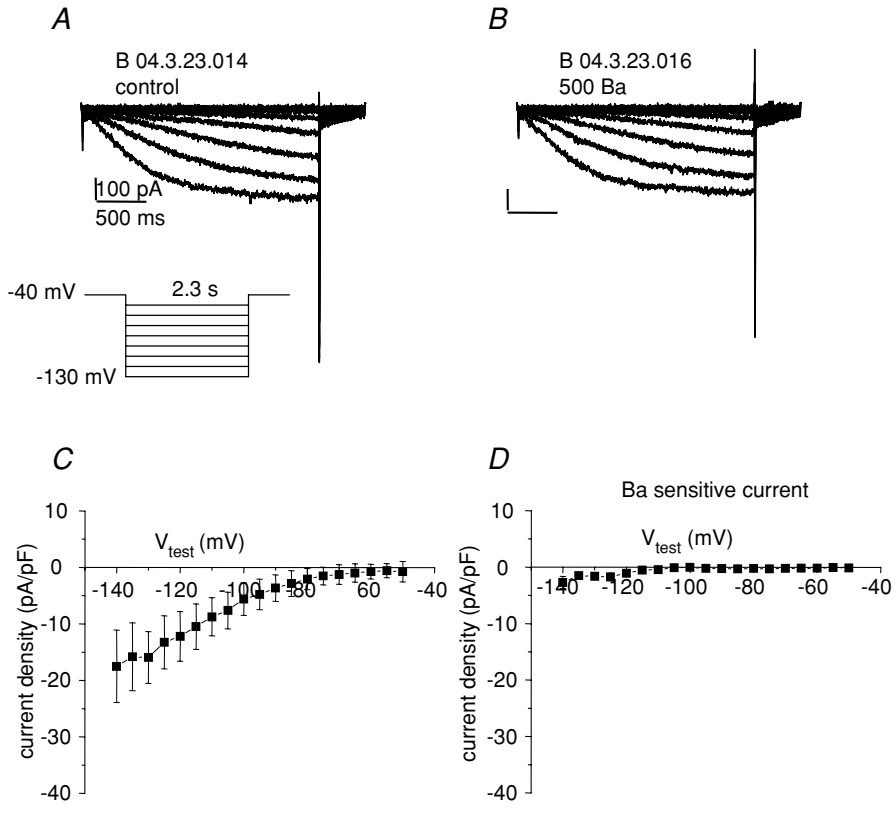

Figure 5. No Kir current is detectable
A, representative single cell, whole-cell patch-clamp recording of current elicited by protocol depicted in the inset in control bath solution. $V_{hold} = -40$ mV, V_{test} for 2.3 s duration to potentials ranging from −50 to −140 mV in 5 mV increments (for clarity currents for 10 mV increments are shown). Inward current is apparent for potentials negative to ~60 mV. *B*, same protocol as *A* in response to 0.5 mM Ba^{2+}. *C*, current–voltage plot for 2.3 s isochronal current in control solution; $n = 6$. *D*, 0.5 mM Ba^{2+}-sensitive 2.3 s isochronal current–voltage relationship. Note the absence of detectable inward rectifier current.

'conditioning' potentials negative to −60 mV. The inset in Fig. 6*A* shows the return step to −40 mV on an expanded scale. The inset in Fig. 6*A* is in essence a 2.3 s 'steady-state' Na^+ channel inactivation protocol with Na^+ current activated by a depolarization to −40 mV. Note that the Na^+ current persists in the presence of Cs^+ ('tail' current in Fig. 6*B*). Although these recordings were made with a relatively slow sample frequency we can still see that the fast inward current is sensitive to the preceding hyperpolarized potential. Thus, the more sustained and more negative the MDP the more HCN will be activated, and the more Na^+ channels will be available (the inverse of inactivated) to open. At 2 mM, Cs^+ did not inhibit spontaneous activity in cell clusters (data not shown). This insensitivity of spontaneous AP activity to Cs^+ argues that HCN may not necessarily contribute to spontaneous depolarization, but the sensitivity to TTX argues that Na^+ current is essential.

The relationship between MDP and the spontaneous maximum upstroke velocity

At steady state, it is difficult to detect ionic current at voltages corresponding to the range between MDP and the AP threshold. The absence of background K^+ currents creates a high input resistance membrane; as a consequence tiny currents can have dramatic effects on membrane potential. This is illustrated in Fig. 7*A*. V_m was recorded from a single cell with an increasing amount of holding current. With only an additional 6 pA of current, from −35 to 41 pA, a noisy V_m recording was converted to a rhythmically beating pattern. For the largest applied holding current we observed increased diastolic intervals; however, during such prolonged intervals we observed subthreshold depolarizations (e.g. asterisk in Fig. 7*A*, bottom centre panel). Increasing holding current induced the following trends (Fig. 7*B*): MDP became more negative, the diastolic interval lengthened and DDR became slower. The slowing of DDR with hyperpolarization is counter-intuitive, given our observation of HCN expression. If HCN were contributing more current more quickly with hyperpolarization we would expect a faster DDR. We can explain the antithesis by considering the notion that Na^+ current dominates diastolic depolarization. It is well established that dV/dt_{max} is an index of Na^+ current (Cohen *et al.* 1984). Therefore, we plotted the MDP *versus* dV/dt_{max} (Fig. 7*C*). This scatter plot shows data from both cell clusters ($n = 14$) and single spontaneously active cells ($n = 3$). First, dV/dt_{max} increases with hyperpolarization. The continuous curve is the Boltzmann distribution with parameters for hES-CM Na^+ current steady-state availability (see below), with the amplitude normalized to the fastest measured spontaneous maximum upstroke velocity. Previous published studies of hES APs (from

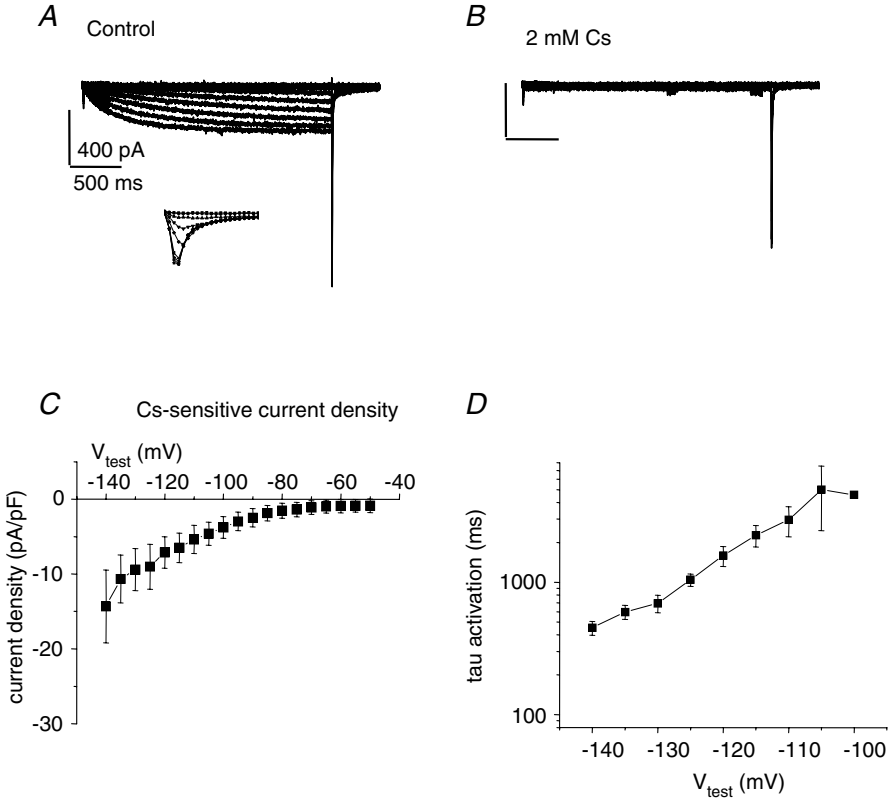

Figure 6. HCN current in hES-CMs
A, representative single cell, whole-cell patch-clamp recording of current elicited by protocol depicted in Fig. 5. Note as in Fig. 5 the slowly developing hyperpolarization-activated current. Also, on the return voltage step to +40 mV a large inward current is activated for $V_{test} > -70$ mV. Inset, expanded time scale of the return step to −40 mV showing inward current. The inward current amplitude upon return to −40 mV is a function of the preceding membrane potential value. The largest inward current amplitude was measured following a −130 mV pulse, while following the −70 mV pulse the current amplitude was approximately half-maximal. *B*, 2 mM Cs^+ induced complete block of slowly developing hyperpolarization-activated current. Note the lack of effect on the rapid inward current activated by the return voltage step to −40 mV *C*, current–voltage plot for 2.3 s isochronal Cs^+−sensitive current. *D*, time course of activation was fitted to a single exponential function; shown is the time constant of activation as a function of V_{test}.

large clusters of cells) showed relatively slow upstroke velocities of $< 10\ V\ s^{-1}$ which corresponds to an MDP of ~ -53 mV in our data. For more negative MDPs, dV/dt_{max} tended to increase, with the highest spontaneous upstroke velocity being about $118\ V\ s^{-1}$.

ES-CM single cell properties: stimulated AP initiation is rapid and TTX sensitive

The absence of Kir in hES cells necessitated the use of a holding current to maintain a V_m in the range of that measured from hES clusters because even gigaohm seals allowed sufficient leak current to artificially depolarize cells. As illustrated in Fig. 7*A*, single cells with hyperpolarized MDPs had prolonged diastolic intervals. By adding a constant holding current we adjusted the MDP to levels ranging from -62 to -70 mV. The long diastolic intervals allowed us to probe the characteristics underlying AP initiation. We stimulated single cells with 1 ms current pulses in 10 pA increments. In stark contrast to mature cardiac preparations, current stimuli of as small as 10–40 pA were sufficient to elicit action potentials (Fig. 8). Figure 8*B* shows part of the trace in Fig. 8*A* on an expanded time base to illustrate the rapid dV/dt_{max} elicited by approximately 120% of stimulus. The rapid dV/dt_{max} is consistent with mature APs. For supra-threshold stimuli, the dV/dt_{max} averaged $118 \pm 14\ V\ s^{-1}$. This value is similar to mature atrial or ventricular myocytes, suggesting a large Na^+ conductance. Therefore we tested the effect of TTX on AP initiation. At 10 μM, TTX blocked single cell AP automaticity, and partially blocked I_{Na} (see below). In cells exposed to TTX, the dV/dt_{max} of stimulated APs was reduced to $38 \pm 15\ V\ s^{-1}$, and three times more current amplitude was required to elicit an AP. The rapid dV/dt_{max} combined with the sensitivity of dV/dt_{max} to TTX argues for the presence of a relatively high Na^+ channel current density. We therefore measured Na^+ current amplitude under voltage clamp. To correlate ion current results with AP properties we measured current in the same cells and under the same ionic conditions as we measured APs. Figure 8*C* shows that there was a positive correlation between Na^+ current amplitude and dV/dt_{max}.

Na^+ current properties suggest functional expression of $Na_V1.5$, the cardiac Na^+ channel

Figure 9*A* shows ionic current elicited by a steady-state inactivation protocol (Fig. 9*A*, inset). A fast inward current peaked within 1.5 ms of depolarization to 0 mV and inactivated with a fast time constant of $\sim$0.5 ms (smooth line superimposed over current trace in Fig. 9*A* and *B*). A slower time constant was needed to fit $< 5\%$ of the total amplitude. These are well-established characteristics of mammalian cardiac Na^+ channel current. TTX blocked I_{Na} and shifted the inactivation curve 10 mV in the hyperpolarizing direction (Fig. 9*C*). Thus, as for $Na_V1.5$ current and native I_{Na}, TTX has apparent higher affinity for inactivated channels in hES-CMs. The mean peak inward, maximally available current density for a test potential (V_{test}) of 0 mV was $-244 \pm 42\ pA\ pF^{-1}$ ($n = 19$ cells). The peak current density of maximally available channels measured from the steady-state inactivation protocol ranged from 69 to $877\ pA\ pF^{-1}$ (Fig. 9*D*). This approximate 10-fold range of current densities is not peculiar to a particular embryoid body, given that from the same EB dissociation we recorded cells in the $800\ pA\ pF^{-1}$ range and cells in the $\sim 100\ pA\ pF^{-1}$ range. The voltage midpoint of steady-state inactivation of Na^+ current is -72.6 ± 0.7 mV ($n = 19$). Figure 9*C* shows pooled, normalized steady-state inactivation curves in control and for TTX. At 100 nM, TTX had no significant effect on current density amplitude; higher doses caused current block and hyperpolarization of the steady-state inactivation midpoint. The half-block concentration of TTX for fully available Na^+ current was 6.6 μM (Fig. 9*E*). The measured IC_{50} is strongly suggestive of $Na_V1.5$ expression.

The high Na^+ channel density poses challenges to accurately measuring fully available I_{Na}, but at the same time it also presents the opportunity of measuring I_{Na} from partially available channels that correspond to MDP. The central goal of the present study was to determine the molecular mechanisms that contribute to spontaneous electrical activity in hES-CMs. With this goal in mind we measured the properties of I_{Na} from a V_{hold} in the range of -60 to -70 mV. Figure 10*A* shows representative I_{Na} elicited by voltage steps ranging from -70 to -10 mV. Increasing depolarization speeded the time to peak and macroscopic inactivation time course. The voltage 'threshold' for I_{Na} activation, when current becomes detectable, was about -50 mV (Fig. 10*B*), and this voltage dependence of activation is well described by a Boltzmann distribution with a midpoint of -30 mV (Fig. 10*B* and *D*). In the range of V_{hold} from -60 to -70 mV the midpoint of activation and the slope of the activation curve are constant (Fig. 10*B*). To further explore the characteristics of hES-CM I_{Na} we fitted the macroscopic inactivation to the sum of two exponentials. For $V_{test} > -10$ mV the fast inactivation time constant (τ_{fast}) fitted $> 90\%$ of the amplitude. The τ_{fast} voltage dependence is shown in Fig. 10*C*. The voltage dependence of τ_{fast} can be described by a single exponential decay with a limiting, voltage-independent rate of 0.44 ms. Thus the activation kinetics and voltage dependencies are consistent with functional $Na_V1.5$ channels. The only exception is that both steady-state inactivation and activation mid-points are shifted in a positive direction on the voltage axis relative to mature preparations (Fig. 10*E*). Moreover, there is overlap of the steady-state inactivation and activation curves (Fig. 10*F*). The potential range of this overlap

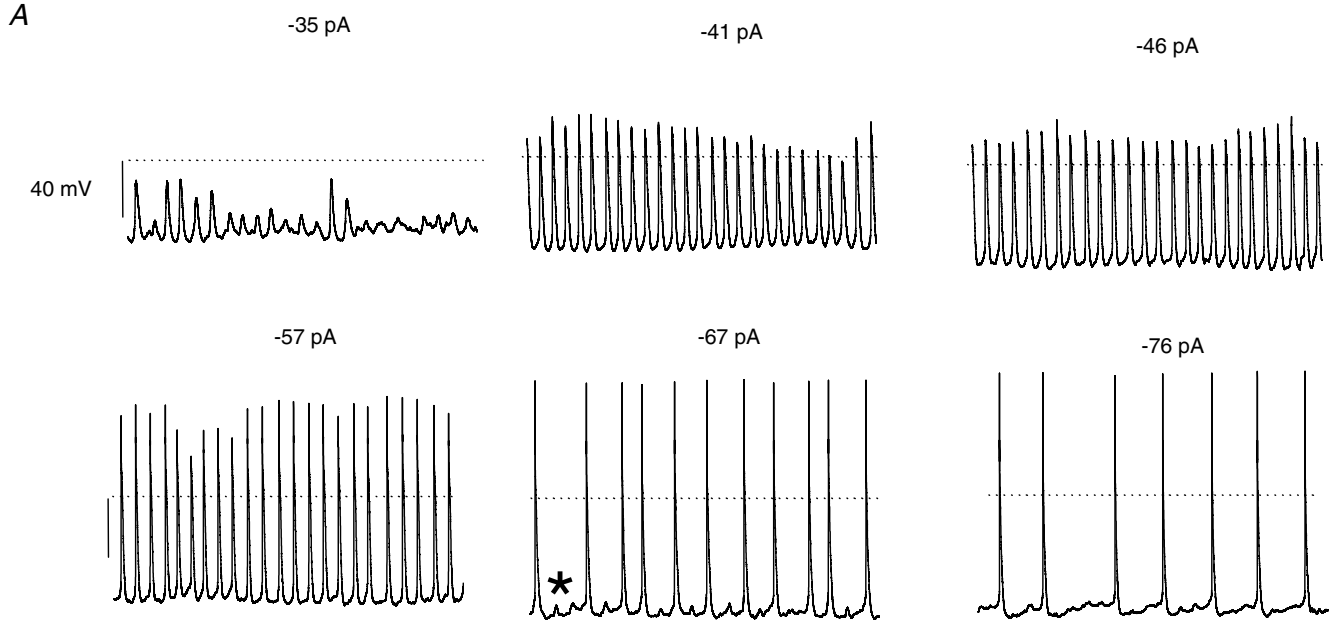

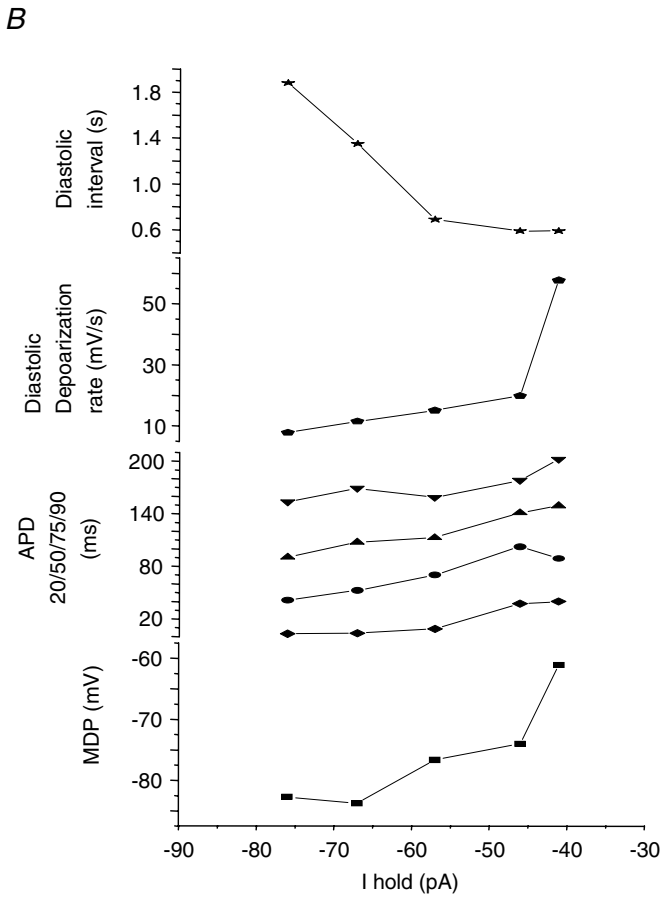

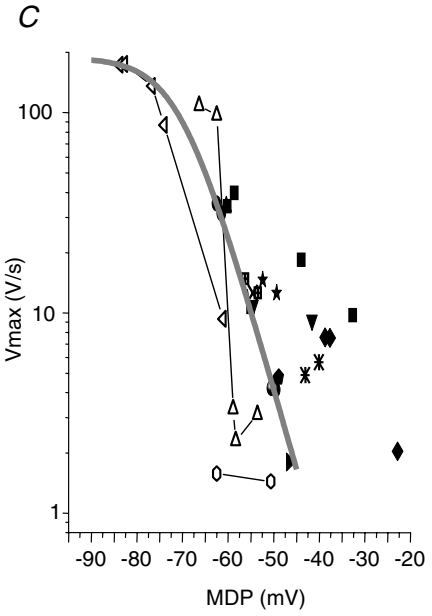

coincides with that of the latter phase of the spontaneous diastolic depolarization, and this latter phase of diastolic depolarization is sensitive to TTX block (Fig. 3). In Fig. 7 we document a window of diastolic potentials that are optimal for spontaneous activity. Taken together, these data suggest that I_{Na} openings within this negative potential range are critical for pacemaking activity.

Na^+ channel recovery from inactivation kinetics underlies refractoriness of excitability of heart tissue. To further characterize hES-CM I_{Na} and to gain a measure of the underpinnings of refractoriness we also measured the recovery from inactivation kinetics of I_{Na}. Figure 11*A* shows representative currents elicited by a test pulse to 0 mV following variable recovery from inactivation duration at −80 mV. We chose this slightly more negative recovery potential for the practical consideration of being able to detect small currents expected from brief recovery intervals. There is a lag of ∼6 ms before fractional recovery can begin to be detectable. The recovery time course is then well described by a bi-exponential function with time constants of 57 and 708 ms.

The I_{Na} kinetics, voltage dependence, and pharmacology strongly suggest the expression of $Na_V1.5$ channels in hES-CMs. Similarly, the Cs^+ sensitivity, kinetics and voltage dependence suggest expression of HCN channels. RT-PCR of hES cDNA demonstrated expression of $Na_V1.5$, HCN-2, and $Ca_V1.2$ (Fig. 12). Furthermore, we were not able to detect $Ca_V1.3$ or HCN-4 mRNA expression. Interestingly, and consistent with the electrophysiological signature, we could detect no Kir2.1, and relatively weak expression of Kir2.3. In summary, the expression of $Na_V1.5$ mRNA is consistent with the relatively high Na^+ current density and the sensitivity of spontaneous excitability to Na^+ channel blockade.

Discussion

This study is the first description of ion channel current recordings from isolated human ES-derived cardiac myocytes (hES-CMs). We focused on voltage-gated Na^+ channel currents because of the sensitivity of spontaneous beating and AP propagation to TTX, and the prominent expression of I_{Na}. Electrical activity of hES-CMs is sensitive to TTX at concentrations known to block the cardiac Na^+ channel $Na_V1.5$. The major finding of this study is that at ∼25 days of differentiation hES-CMs exhibit a hybrid developmental excitable phenotype. In common with early embryonic heart myocytes, hES-CMs have no detectable Kir current, but express a prominent I_{Na} approaching levels comparable to those measured from mature cardiac preparations.

The basis for automaticity

The ionic currents of hES-CMs in this study are consistent with a hybrid, or intermediate stage of embryonic development. In animal models during ontogeny there is a progressive increase of I_{Na} (Nathan & DeHaan, 1978) and inward rectifier currents in atrial and ventricular myocytes (Davies *et al.* 1996). Ca^{2+} channel currents appear early in development and are largely responsible for the relatively slow dV/dt_{max} of the action potential. The paucity of inward rectifier channels creates a high input resistance surface membrane. As a consequence only a few open channels allowing either Na^+ or Ca^{2+} flux may be sufficient to bring the developing heart cell to AP threshold. A similar pattern is also reproduced in mouse ES cells (Maltsev *et al.* 1994). Data on human fetal development is scarce; however, this same trend apparently also exists (Tuganowski & Tendera, 1973; Janse *et al.* 1976). In our study, the low current stimulus threshold for AP initiation, and the rapid upstroke velocity coupled with the pharmacological evidence for Na^+, but not Ca^{2+} channel sensitivity argues for a prominent role of $Na_V1.5$ channels in the spontaneous excitability of hES-CMs. The high Na^+ current density is indicative of more mature heart cells whereas the high input resistance is more typical of immature cells. The low background conductance facilitates AP production with only a small number of open $Na_V1.5$ channels. Based on the present study we would predict that hES-CMs of up to 30 days differentiation would be good pacemakers, but without Kir expression pose a pro-arrhythmic risk.

In the early developing mouse myocardium, in contrast to hES-CMs, it is thought that pacemaker cells among the embryonic cardiomyocytes start with a 'primitive' pacemaker AP that is probably generated by only two ionic currents, $I_{Ca,L}$ and $I_{K,to}$ (Hescheler *et al.* 1997), or even just by intracellular Ca^{2+} oscillations(Viatchenko-Karpinski *et al.* 1999). Subsequent to this primitive pacemaker stage HCN knockout in mice suggests an essential role for HCN-4 in maintaining heart development

Figure 7. Spontaneous AP generation corresponds to a window of voltages that corresponds to the overlap of Na^+ channel activation and inactivation

A, representative single cell APs recorded from the whole-cell configuration. The amplitude of constant holding current is listed above each subpanel. Dotted line is 0 mV; scale bar 40 mV 15 s of continuous data shown for each panel. Asterisk in bottom centre panel shows typical 'failed' AP initiation. *B*, AP parameters plotted as a function of holding current for cell shown in *A*. *C*, pooled data from 3 single cells and 14 cell cluster recordings. Individual symbol types depict separate recordings. V_{max} is plotted as a function of MDP. The smooth grey line is a Boltzmann distribution with a midpoint of −72.5 mV, a slope of 5.4 and a maximum of 118.

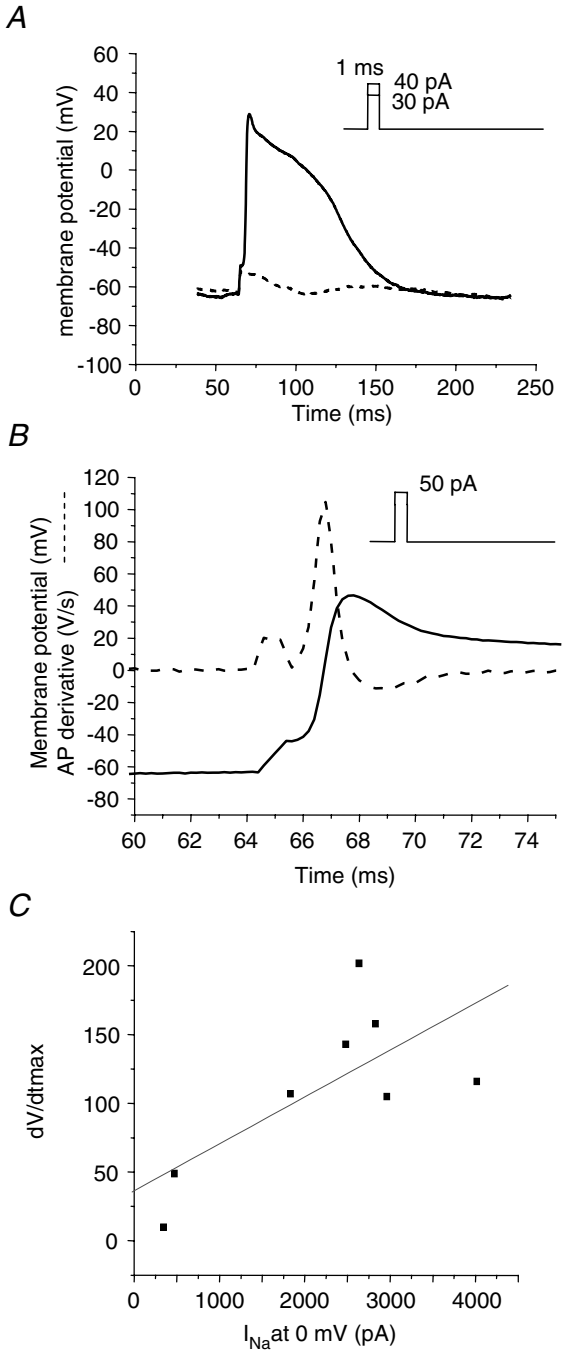

Figure 8. Single cell APs are stimulated with small, brief current pulses
A, representative AP elicited by a 1 ms duration, 40 pA current injection (continuous line) superimposed on the V_m response to a subthreshold stimulus (dashed line). Constant holding current maintained MDP ∼−65 mV (29 pA in this example). *B*, a supra-threshold stimulus (50 pA) elicits an AP upstroke (continuous line) with a rapid V_{max}. Dashed line superimposed on AP is the AP derivative to illustrate dV/dt_{max} (V_{max}). Note the expanded time scale relative to *A* to illustrate rate of rise of AP. *C*, a subset of 9 cells in which Na^+ current was recorded following single cell APs. V_{max} is plotted as a function of Na^+ current. Linear regression $(R) = 0.71$.

(Stieber *et al.* 2003). Similarly, intracellular Ca^{2+} may be essential for pacemaker dominance in mature pacemaker cells (Lakatta *et al.* 2003). Our data do not exclude a contribution of HCN or $I_{Ca,L}$ to the upstroke, but we do show evidence that HCN or $I_{Ca,L}$ activity is not a requirement for spontaneous AP upstroke initiation. We clearly show that AP autorhythmicity is insensitive to Cs^+ or nifedipine, but is sensitive to TTX block of I_{Na}. Therefore, we conclude that the human ES-CM AP initiation is fundamentally different from that of the well-studied mouse.

$Na_V1.5$ underlies hES-CM I_{Na}

In mature cardiac preparations pacemaker cells are spontaneously active due to a mixture of ion channel expression that includes $I_{Ca,L}$, I_f (HCN), and the absence of significant Kir expression. Recently, studies have shown that a TTX-sensitive Na^+ channel (1–10 nM TTX) also contributes to spontaneous AP initiation (Maier *et al.* 2003). In hES-CMs we show, however, that I_{Na} is unaffected by 100 nM TTX. The TTX half-block concentration is 6.6 μM, which is very close to the widely cited range of 1–6 μM for half-block of native and cloned human Na^+ current (Fozzard & Hanck, 1996). In fact, in adult human myocytes 10 μM TTX was required for half-block of I_{Na} (Schneider *et al.* 1994). Some of the discrepancies in reported half-block concentrations of TTX can arise from the protocol dependence of the degree of block. TTX block of Na^+ channels is sensitive to both external Na^+ concentration and channel state dependence (Fozzard & Hanck, 1996). It is likely that the Na^+ dependence arises from competition between the guanidinium group of the toxin and the partially dehydrated permeating Na^+ ion (reviewed by Fozzard & Hanck, 1996). We worked with relatively high external Na^+ which may partially explain the relatively weak TTX sensitivity of hES-CM I_{Na}. The state dependence of TTX block may help to explain the tendency for TTX to have a greater effect on spontaneous excitability than would be anticipated from the measured half-block concentration of maximally available I_{Na} (Fig. 9). It should be noted that early reports of dissociation equilibrium constants for TTX block of native cardiac I_{Na} showed an almost 5-fold increase in apparent TTX affinity for inactivated *versus* closed state channels (Carmeliet, 1987). This finding was later confirmed in cloned, heterologously expressed cardiac Na^+ channels (Satin *et al.* 1992). One consequence of this higher affinity TTX block is that TTX will have an apparent higher affinity for intact hES-CMs by virtue of the fact that depolarized holding potentials promote substantial channel inactivation. Given that MDP was never more negative than −65 mV, this implies that in intact hES-CMs the majority of Na^+

channels are steady-state inactivated. Hence, lower TTX concentrations than that required for the fully available half-block level are required to inhibit spontaneous AP initiation.

The voltage dependence and kinetics of hES-CM I_{Na} are also consistent with the function of the human $Na_V1.5$ channel, with some minor, but notable exceptions. hES-CM I_{Na}, native human I_{Na}, and heterologously expressed cloned human $Na_V1.5$ current all display an approximate 43 mV difference between the midpoints for macroscopic activation and steady-state inactivation. It is notable, however, that hES-CM activation and inactivation midpoints are uniformly shifted ∼15 mV in the depolarized direction relative to their mature counterparts. It is unlikely that this shift is due to a unique polymorphism in the hES line in this report. Consider, for example, that a careful study of the functional characteristics of polymorphisms of $Na_V1.5$ variants showed that different polymorphisms confer different expression levels but similar voltage dependencies (Makielski *et al.* 2003). Moreover, early studies in developing mammalian myocardium noted that I_{Na} is present in the earliest beating heart, increases in amplitude with development, and has unchanged kinetics, pharmacology or voltage dependencies with the exception of a progressive hyperpolarizing shift of steady-state inactivation and activation as a function of development (Shigenobu & Sperelakis, 1971; Sperelakis & Shigenobu,

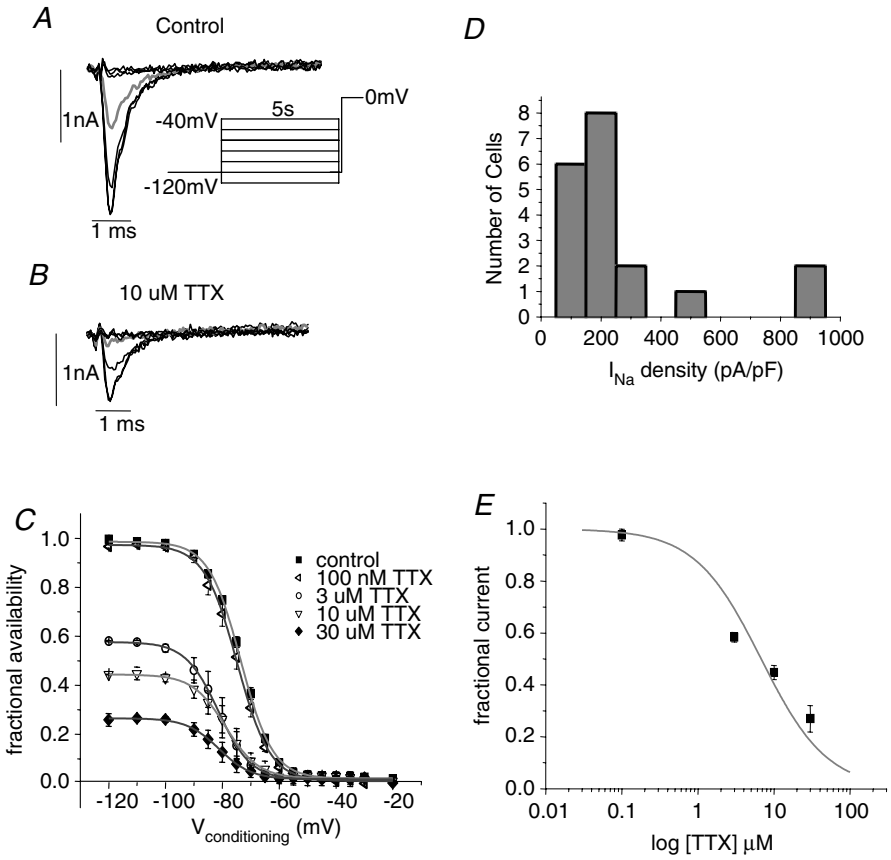

Figure 9. Steady-state inactivation and TTX blockade of hES-CM I_{Na} are similar to that for cardiac Na^+ channels

A, current traces elicited by a test potential step to 0 mV following 5 s conditioning steps to −120, −100, −80, −70, −60, −50 and −40 mV under control ionic conditions. Grey current trace is for conditioning voltage step to −70 mV. *B*, same voltage protocol and same current traces shown as in *A*, but in the presence of 3 μM TTX. Grey trace is also the current elicited following a conditioning step to −70 mV. *C*, normalized steady-state inactivation curve in control bath and for TTX concentrations as indicated; $n = 12$. Smooth line is Boltzmann distribution with the following values for half-activation ($V_{1/2}$) and slope factors (k): control (■), −73 mV and 5.6; 0.1 μM TTX (◁), −74 mV and 5.8; 3 μM TTX (○), −81 mV and 5.8; 10 μM TTX (▽), −79 mV and 5.8; 30 μM TTX (♦), −81 mV and 5.7. *D*, distribution of current density of cells from peak current obtained from the steady-state inactivation protocol. Bin width is 100 pA pF^{-1}. *E*, TTX dose–response relationship fitted with a single site blocking curve of the form: fractional block $= 1/(1 + [TTX]/K_d)$ with $K_d = 6.8$ μM.

1972; Lompre *et al.* 1979; Fujii *et al.* 1988; Sada *et al.* 1995). Thus the early embryonic shift of I_{Na} is possibly due to an uncharacterized splicevariation or accessory subunit expression in hES cells, and this would form an interesting basis for future investigations. Finally, although a uniform translation of voltage dependence can be explained by a charge-screening mechanism that would be unique to the embryonic cellular membrane

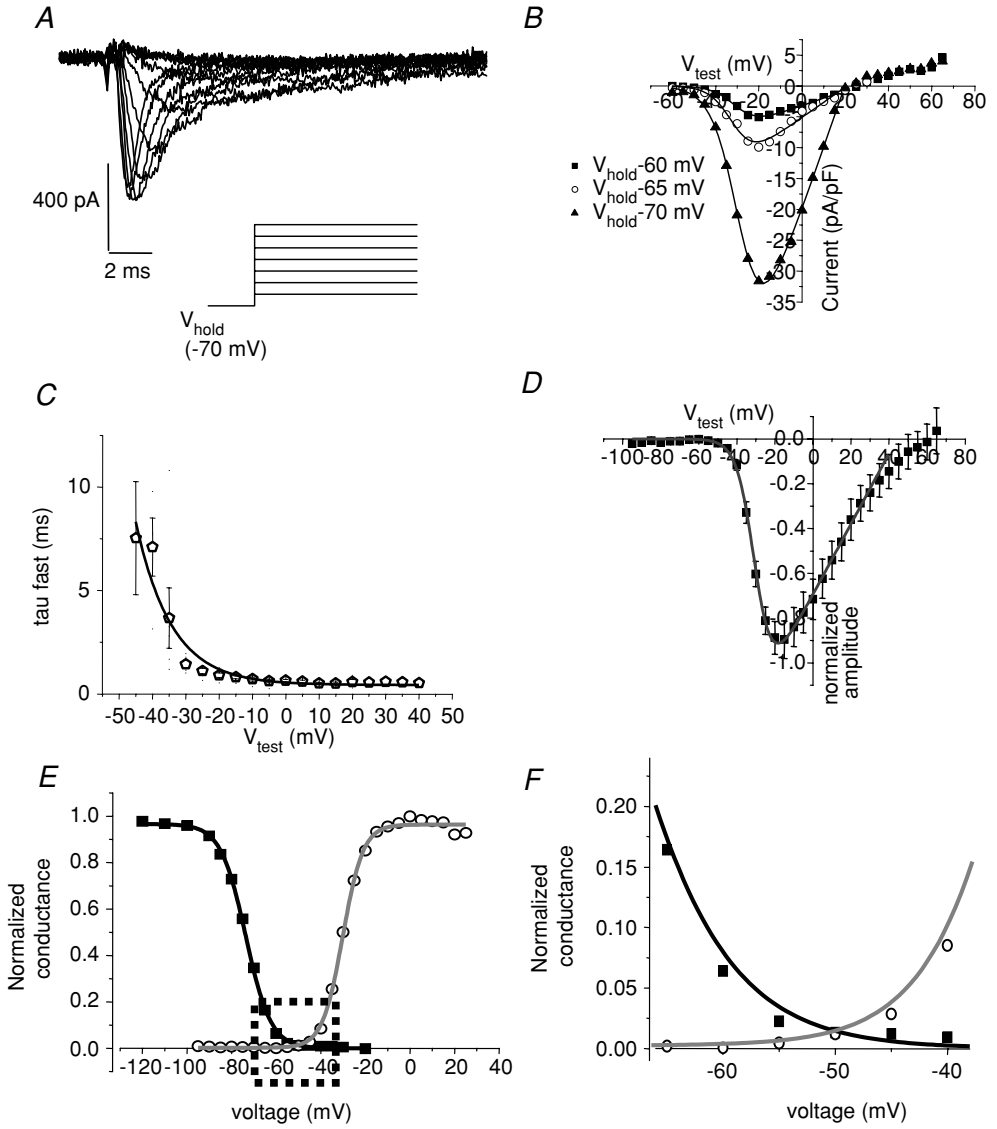

Figure 10. I_{Na} in response to increasing depolarizations
A, current traces elicited from V_{hold} −70 mV to depolarizations ranging from −60 to −5 mV in 5 mV increments in a representative cell. *B*, current–voltage relationship for peak inward current of a representative cell for V_{hold} −60 (■), −65 (○), and −70 mV (▲). Smooth curve is a modified Boltzmann distribution where, $G(V) = G_{max}(V_{test} - E_{rev}))/\{1 + \exp((V_{1/2} - V_{test})/k\}$, with half-activation ($V_{1/2}$) and slope factors ($k$) of −30 mV and 5.2 for $V_{hold} = -60$ mV; −31 mV and 5.1 for $V_{hold} = -65$ mV; −29 mV and 5.9 for $V_{hold} = -70$ mV. *C*, macroscopic current decay was fitted to a bi-exponential function. τ_{fast} is plotted as a function of test potential (V_{test}). Curve is a single exponential fit of τ_{fast} with a maximum rate of 0.4 ms. *D*, normalized pooled data for peak inward current elicited by various test potentials. Smooth curve is a modified Boltzmann distribution with $V_{1/2} = -30$ mV, $k = 4.6$, and $E_{rev} = 44$ mV; $n = 21$. *E*, conductance transform of *D* (activation curve, grey line) superimposed on the normalized peak steady-state inactivation curve from Fig. 9*C*. Dashed box indicates approximate boundaries of the potential range for diastolic depolarization. *F*, expanded view of the dashed box in *E* to illustrate the overlapping window of potentials where Na^+ channels may simultaneously activate and are partially available to activate.

we think that this possibility is unlikely because the Cs^+-sensitive HCN current exhibited a similar voltage dependence to that measured from mature human Purkinje fibre and ventricular myocytes (Han *et al.* 2002). Thus there is not a common shift towards depolarized potentials of all voltage-activated ionic conductances in hES-CMs. Regardless of the mechanism, the shift in voltage dependency towards depolarized potentials allows Na^+ channels to operate in the relatively, in comparison to mature working cardiac myocytes, depolarized range of the embryonic MDP.

Kinetic parameters of hES-CM I_{Na} compared to human I_{Na} are also similar. Our measures of a fast inactivation rate of ∼0.4 ms at 28°C for test steps positive to 0 mV is close to values ranging from 0.2 to 0.4 ms obtained from heterologously expressed human $Na_V1.5$ channels at 22°C at ∼0.35 ms and at the relatively elevated temperature of 32°C (Nagatomo *et al.* 1998; Dumaine *et al.* 1999). A consequence of the shift of the hES-CM I_{Na} gating is that kinetic parameters are also shifted. A key parameter to consider for the maintenance of spontaneous pacing is the rate of recovery from inactivation. However, for the purpose of comparison with the literature the values obtained need to be normalized to the inactivation midpoint; in our case this is slightly less than 10 mV hyperpolarized to the inactivation midpoint. For example, in a careful study of canine ventricle in which the recovery potential was varied, the recovery from inactivation was described by two time constants with rates of 116 and 454 ms (Pu & Boyden, 1997). These recovery rates are sufficient to allow > 80% of channels to recover during a 1 s interpulse interval. This slow recovery from inactivation is consistent with creating a limit to the rapidity of spontaneous ES cell beating.

Comparison to murine ES-derived heart cells

Because the mouse is an important species for designing human disease models it is important to compare the ionic currents between murine and human ES-derived cardiac myocytes. In terminally differentiated mouse ES-CMs the I_{Na} current density was ∼200 pA pF^{-1} in one study, but only ∼70 pA pF^{-1} in a more recent report (Fijnvandraat *et al.* 2003). We now show that human ES-CMs express a range of current densities between over 800 and 60 pA pF^{-1} with an average of 242 pA pF^{-1}. The large disparity between mouse and human gestation periods must be considered. In the mouse 22 days of mES cell plating time is taken as terminal differentiation; a comparable duration in humans would be ∼270 days. In this study, we measured I_{Na} from hES cells between 18 and 35 days after plating of embryoid bodies. During this window of time we noted more disparity of current density within cells from a single embryoid body dissociation than between cells of different ages. If we simply scale human time to mouse time based on *in utero* gestation periods, our study would represent a cell differentiation period of about 1.3 mouse-days and would coincide approximately with mouse-days 2–3 of ES differentiation time (starting from

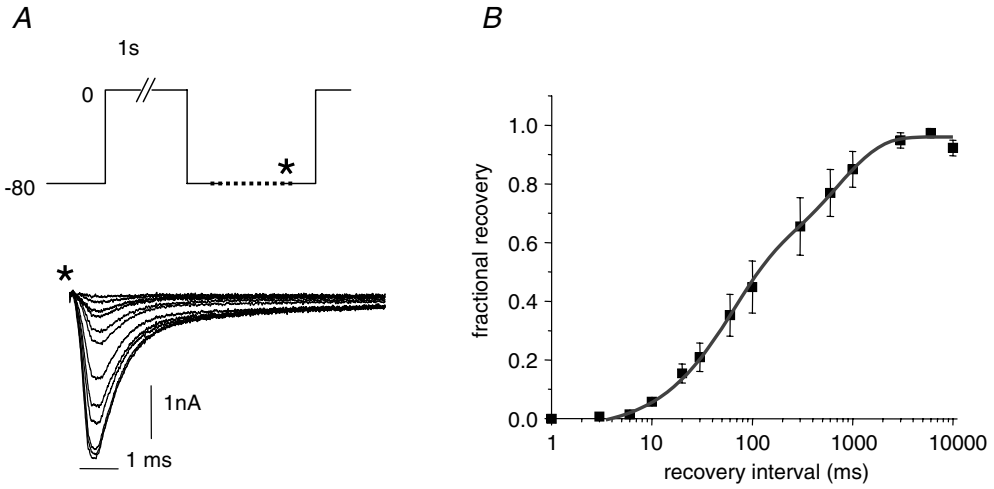

Figure 11. Time course of recovery from inactivation of I_{Na}
A, schematic diagram of protocol used to assess recovery from inactivation. Cell was returned to −80 mV for a variable duration following a 1 s depolarization to 0 mV. Data acquisition was initiated as indicated by asterisk. Representative current traces elicited by final test step to 0 mV for recovery intervals listed in the graph in *B*. Scale bars 1 ms and 1 nA. *B*, pooled, normalized recovery from inactivation data is fitted by a bi-exponential function with time constants of 57 ms (55% of the amplitude) and 457 ms (45% of the amplitude). Peak current was normalized to current recovery following a 10 s interpulse interval.

the plating of embryoid bodies). Prior to 5 mouse-days of differentiation time murine ES-CMs expressed no detectable I_{Na} (Maltsev *et al.* 1994; Fijnvandraat *et al.* 2003). We highlight these differencessimply to make the point that the hES I_{Na} density is extremely high for such a relatively early developmental time. Similarly, HCN current (I_f) density in human ES-CMs at a stage equivalent to only 2–3 mouse-days of differentiation were comparable to the 1–10 pA pF^{-1} levels measured from terminally differentiated mouse ES-CMs (> 12 mouse-days; (Maltsev *et al.* 1994). The human development of Kir (I_{K1}) may also parallel that of mouse. In the mouse, Kir expression does not appear until the terminal differentiation stage (16 mouse-days). As in the mouse, we cannot detect Kir expression in human ES-CMs at a stage equivalent to 3–4 mouse-days of differentiation. To extend the parallel in humans, we anticipate having to investigate human ES-CM cultures over 200 days after plating in order to observe Kir expression. Such a time frame entails obvious technical and practical limitations. On the other hand, the relatively long human gestation period presents the opportunity to carefully evaluate the physiological mechanisms of human heart cell early development in future studies.

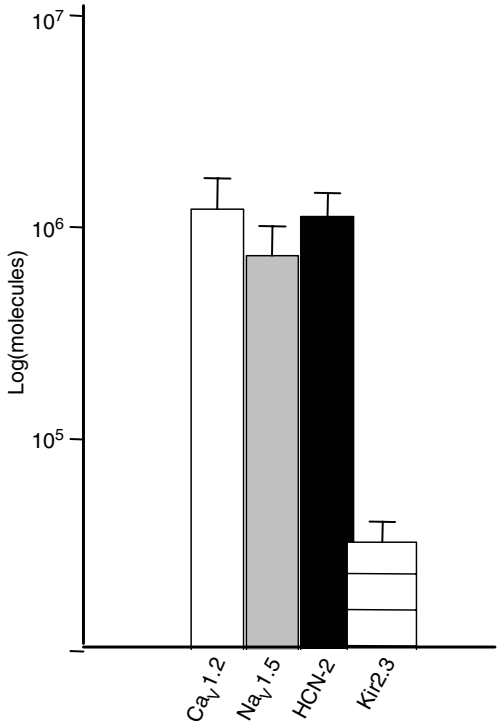

Figure 12. RT-PCR analysis of hES expression of ion channel mRNA
We detected similar expression of RNA encoding $Na_V1.5$, $Ca_V1.2$, and HCN2. A much weaker signal for Kir2.3 was observed. In contrast, we could not detect $Ca_V1.3$, Kir2.1 or HCN-4. Primer sequences and accession numbers are listed in Table 1.

Although we cannot access early human hearts for study for obvious ethical reasons, in the mouse ES-CMs parallel native development (Doevendans *et al.* 2000), which reinforces our proposal that hES-CMs differentiating *in vitro* provide a good model for early human development.

Comparison to earlier human ES studies

There are no reports of ionic currents in hES-CMs, but there are two published reports of hES-CM APs from cell clusters. All of our AP recordings have a definitive plateau and they are similar to the embryonic ventricular-like action potentials reported by He *et al.* (2003), even though their experiments were carried out at 37°C. We report a dV/dt_{max} (118 V s^{-1}) from isolated cells that is markedly faster than the dV/dt_{max} in cell clusters, ~8 V s^{-1} (He *et al.* 2003; Mummery *et al.* 2003). There are several important factors to consider in explaining this discrepancy. First, our voltage-clamp recordings of a prominent I_{Na} coupled with TTX sensitivity of spontaneous excitability and conduction furnishes proof that the Na^+ channel ($Na_V1.5$) is the dominant ion charge carrier driving the upstroke of the AP. Therefore, the MDP is a critical determinant of Na^+ channel availability, which in turn is a critical determinant of maximum upstroke velocity (Fozzard *et al.* 1987; Sheets *et al.* 1988). Second, AP propagation and morphology are dependent on both active and passive properties. In modelling and experimental studies, dV/dt_{max} increases with cell uncoupling (Rudy & Quan, 1987; Shaw & Rudy, 1997). EBs show uniform TTX sensitive conduction velocity (see Fig. 1 and Kehat *et al.* 2002) that is sensitive to conduction block by gap junction uncoupling reagents (I. Kehat & L. Gepstein, unpublished observations). Thus cell–cell coupling is relatively strong. These conditions are therefore expected to reduce dV/dt_{max} relative to isolated cells which are small and coupled to no other active or passive electrical components. In both single cells and well-coupled clusters, slight deviations in MDP will have large effects on Na^+ channel inactivation. Finally, we voltage-clamped isolated cells based on spontaneous beating and morphology and thus introduced a potential selection bias.

Summary

In conclusion, this study is the first to measure and characterize ionic currents and single cell AP properties from isolated human ES cells. TTX inhibits the automatic excitability of clusters of cardiac myocytes in EBs, and that of isolated cells. The high input resistance coupled with a high Na^+ channel density creates conditions for spontaneous excitability.

References

Amit M, Carpenter MK, Inokuma MS, Chiu CP, Harris CP, Waknitz MA, Itskovitz-Eldor J & Thomson JA (2000). Clonally derived human embryonic stem cell lines maintain pluripotency and proliferative potential for prolonged periods of culture. *Dev Biol* **227**, 271–278.

Bustin SA (2002). Quantification of mRNA using real-time reverse transcription PCR (RT-PCR): trends and problems. *J Mol Endocrinol* **29**, 23–39.

Carmeliet E (1987). Voltage-dependent block by tetrodotoxin of the sodium channel in rabbit cardiac Purkinje fibers. *Biophys J* **51**, 109–114.

Cohen CJ, Bean BP & Tsien RW (1984). Maximal upstroke velocity as an index of available sodium conductance. Comparison of maximal voltage clamp measurements of sodium current in rabbit Purkinje fibers. *Circulation Res* **54**, 636–651.

Davies MP, An RH, Doevendans P, Kubalak S, Chien KR & Kass RS (1996). Developmental changes in ionic channel activity in the embryonic murine heart. *Circ Res* **78**, 15–25.

DeHaan RL (1980). Differentiation of excitable membranes. *Current Topics Dev Biol* **16**, 117–164.

DeHaan RL & Gottlieb SH (1968). The electrical activity of embryonic chick heart cells isolated in tissue culture singly or in interconnected cell sheets. *J General Physiol* **52**, 643–665.

Doevendans PA, Kubalak SW, An RH, Becker DK, Chien KR & Kass RS (2000). Differentiation of cardiomyocytes in floating embryoid bodies is comparable to fetal cardiomyocytes. *J Mol Cell Cardiol* **32**, 839–851.

Dumaine R, Towbin JA, Brugada P, Vatta M, Nesterenko DV, Nesterenko VV, Brugada J, Brugada R & Antzelevitch C (1999). Ionic mechanisms responsible for the electrocardiographic phenotype of the brugada syndrome are temperature dependent. *Circ Res* **85**, 803–809.

Feld Y, Melamed-Frank M, Kehat I, Tal D, Marom S & Gepstein L (2002). Electrophysiological modulation of cardiomyocytic tissue by transfected fibroblasts expressing potassium channels: a novel strategy to manipulate excitability. *Circulation* **105**, 522–529.

Fijnvandraat AC, van Ginneken AC, de Boer PA, Ruijter JM, Christoffels VM, Moorman AF & Lekanne Deprez RH (2003). Cardiomyocytes derived from embryonic stem cells resemble cardiomyocytes of the embryonic heart tube. *Cardiovasc Res* **58**, 399–409.

Fozzard HA & Hanck DA (1996). Structure and function of voltage dependent sodium channels: comparison of rat brain II and cardiac isoforms. *Physiol Rev* **76**, 887–926.

Fozzard HA, Hanck DA & Sheets MF (1987). The relationship between V{-max} and I{-Na} in cardiac Purkinje cells and their interpretation from single Na{++} analysis. In *Moleclular and Cellular Mechanisms of Antiarrhythmic Agents*, ed. Hondeghem LM, pp. 1–8. Hondeghem, LM, Nashville.

Fujii S, Ayer RK Jr & DeHaan RL (1988). Development of the fast sodium current in early embryonic chick heart cells. *J Membr Biol* **101**, 209–223.

Gepstein L (2002). Derivation and potential applications of human embryonic stem cells. *Circ Res* **91**, 866–876.

Han W, Zhang L, Schram G & Nattel S (2002). Properties of potassium currents in Purkinje cells of failing human hearts. *Am J Physiol Heart Circ Physiol* **283**, H2495–2503. Epub 2002 August 2415.

He JQ, Ma Y, Lee Y, Thomson JA & Kamp TJ (2003). Human embryonic stem cells develop into multiple types of cardiac myocytes. Action potential characterization. *Circ Res* **5**, 5.

Hescheler J, Fleischmann BK, Lentini S, Maltsev VA, Rohwedel J, Wobus AM & Addicks K (1997). Embryonic stem cells: a model to study structural and functional properties in cardiomyogenesis. *Cardiovasc Res* **36**, 149–162.

Hescheler J, Fleischmann BK, Wartenberg M, Bloch W, Kolossov E, Ji G, Addicks K & Sauer H (1999). Establishment of ionic channels and signalling cascades in the embryonic stem cell-derived primitive endoderm and cardiovascular system. *Cells Tissues Organs* **165**, 153–164.

Hille B (2001). *Ion Channels of Excitable Membranes*. Sinauer Associates, Inc, Sunderland, MA.

Janse MK, Anderson RH, van Capelle FJ & Durrer D (1976). A combined electrophysiological and anatomical study of the human fetal heart. *Am Heart J* **91**, 556–562.

Kehat I & Gepstein L (2003). Human embryonic stem cells for myocardial regeneration. *Heart Fail Rev* **8**, 229–236.

Kehat I, Gepstein A, Spira A, Itskovitz-Eldor J & Gepstein L (2002). High-resolution electrophysiological assessment of human embryonic stem cell-derived cardiomyocytes: a novel in vitro model for the study of conduction. *Circ Res* **91**, 659–661.

Kehat I, Kenyagin-Karsenti D, Snir M, Segev H, Amit M, Gepstein A, Livne E, Binah O, Itskovitz-Eldor J & Gepstein L (2001). Human embryonic stem cells can differentiate into myocytes with structural and functional properties of cardiomyocytes. *J Clin Invest* **108**, 407–414.

Lakatta EG, Maltsev VA, Bogdanov KY, Stern MD & Vinogradova TM (2003). Cyclic variation of intracellular calcium: a critical factor for cardiac pacemaker cell dominance. *Circ Res* **92**, e45–50.

Lompre AM, Poggioli J & Vassort G (1979). Maintenance of fast Na-channels during primary culture of embryonic chick heart cells. *J Mol Cell Cardiol* **11**, 813–825.

McDonald TF, Sachs HG & DeHaan RL (1973). Tetrodotoxin desensitization in aggregates of embryonic chick heart cells. *J General Physiol* **62**, 286–302.

Maier SK, Westenbroek RE, Yamanushi TT, Dobrzynski H, Boyett MR, Catterall WA & Scheuer T (2003). An unexpected requirement for brain-type sodium channels for control of heart rate in the mouse sinoatrial node. *Proc Natl Acad Sci U S A* **100**, 3507–3512. Epub 2003 March 3511.

Makielski JC, Ye B, Valdivia CR, Pagel MD, Pu J, Tester DJ, Ackerman MJ, Nagatomo T, Fan Z, Tonkovich GS, January CT & Kyle JW (2003). A ubiquitous splice variant and a common polymorphism affect heterologous expression of recombinant human SCN5A heart sodium channels. *Circ Res* **93**, 821–828.

Maltsev VA, Wobus AM, Rohwedel J, Bader M & Hescheler J (1994). Cardiomyocytes differentiated in vitro from embryonic stem cells developmentally express cardiac-specific genes and ionic currents. *Circ Res* **75**, 233–244.

Mummery C, Ward-van Oostwaard D, Doevendans P, Spijker R, van den Brink S, Hassink R, van der Heyden M, Opthof T, Pera M, de la Riviere AB, Passier R & Tertoolen L (2003). Differentiation of human embryonic stem cells to cardiomyocytes: role of coculture with visceral endoderm-like cells. *Circulation* **107**, 2733–2740.

Nagatomo T, Fan ZYeB, Tonkovich GS, January CT, Kyle JW & Makielski JC (1998). Temperature dependence of early and late currents in human cardiac wild-type and long Q-T DeltaKPQ Na^+ channels. *Am J Physiol* **275**, H2016–H2024.

Nathan RD & DeHaan RL (1978). In vitro differentiation of a fast Na^+ conductance in embryonic heart cell aggregates. *Proc Natl Acad Sci U S A* **75**, 2776–2780.

Pu J & Boyden PA (1997). Alterations of Na currents in myocytes from epicardial border zone of the infarcted heart. *Circulation Res* **81**, 110–119.

Rudy Y & Quan WL (1987). A model study of the effects of the discrete cellular structure on electrical propagation in cardiac tissue. *Circ Res* **61**, 815–823.

Sachinidis A, Fleischmann BK, Kolossov E, Wartenberg M, Sauer H & Hescheler J (2003). Cardiac specific differentiation of mouse embryonic stem cells. *Cardiovasc Res* **58**, 278–291.

Sada H, Ban T, Fujita T, Ebina Y & Sperelakis N (1995). Developmental change in fast Na channel properties in embryonic chick ventricular heart cells. *Can J Physiol Pharmacol* **73**, 1475–1484.

Satin J, Kyle JW, Chen M, Bell P, Cribbs LL, Fozzard HA & Rogart RB (1992). A mutant of TTX-resistant cardiac sodium channels with TTX-sensitive properties. *Science* ***256***, 1202–1205.

Schneider M, Proebstle T, Hombach V, Hannekum A & Rudel R (1994). Characterization of the sodium currents in isolated human cardiocytes. *Pflugers Arch* **428**, 84–90.

Shaw RM & Rudy Y (1997). Ionic mechanisms of propagation in cardiac tissue. Roles of the sodium and L-type calcium currents during reduced excitability and decreased gap junction coupling. *Circ Res* **81**, 727–741.

Sheets MF, Hanck DA & Fozzard HA (1988). Nonlinear relationship between Vmax and I_{Na} in canine cardiac Purkinje cells. *Circ Res* **63**, 386–398.

Shigenobu K & Sperelakis N (1971). Development of sensitivity to tetrodotoxin of chick embryo hearts with age. *J Mol Cellular Cardiol* **3**, 271–286.

Sperelakis N (1984). Developmental changes in membrane electric properties of the heart. In *Physiology and Pathophysiology of the Heart*, ed. Sperelakis N, pp. 543–573. M. Nijhoff, Boston.

Sperelakis N & Shigenobu K (1972). Changes in membrane properties of chick embryonic hearts during development. *J General Physiol* **60**, 430–453.

Stieber J, Herrmann S, Feil S, Loster J, Feil R, Biel M, Hofmann F & Ludwig A (2003). The hyperpolarization-activated channel HCN4 is required for the generation of pacemaker action potentials in the embryonic heart. *Proc Natl Acad Sci U S A* **100**, 15235–15240.

Tuganowski W & Tendera M (1973). Components of the action potential of human embryonic auricle. *Am J Physiol* **224**, 803–808.

Viatchenko-Karpinski S, Fleischmann BK, Liu Q, Sauer H, Gryshchenko O, Ji GJ & Hescheler J (1999). Intracellular Ca^{2+} oscillations drive spontaneous contractions in cardiomyocytes during early development. *Proc Natl Acad Sci U S A* **96**, 8259–8264.

Whelan JA, Russell NB & Whelan MA (2003). A method for the absolute quantification of cDNA using real-time PCR. *J Immunol Meth* **278**, 261–269.

Acknowledgements

We gratefully acknowledge the support of the Lady Davis Fellowship Trust (J.S.). This work is also supported in part by NIH grants (J.S.), and by the Israel Science Foundation (grant no. 520/01) and the Nahum Guzik Research Fund (L.G.). We thank the University of Kentucky Vice Chancellor for Research, Del Collins, and the Department of Physiology for providing international travel funding. We thank Harry Fozzard for his insightful comments.